Lavandula Stoechas as a Green Corrosion Inhibitor for Monel 400 in Sulfuric Acid: Electrochemical, Gravimetrical, and AFM Investigations

Kherraf, Sihem*[*+]*

Department of Petrochemicals, University of 20 août 1955-Skikda, Skikda, ALGERIA

Khelfaoui, Malika[•]; Boughaita, Imen [•]

Department of Process Engineering, University of 20 août 1955-Skikda, Skikda, ALGERIA

Marsa, Zoubida[•]; Medjram, Mohamed Salah [•]

Laboratory of Chemical Engineering and Environment of Skikda, University of 20 août 1955-Skikda, Route El-Hadaeik B.P. 26 skikda, ALGERIA

ABSTRACT: *The inhibiting effect of Lavendula stoechas extract on the corrosion of Monel alloy 400 in 0.5 M sulfuric acid at different temperatures (298–328 K) was evaluated by mass loss measurements and electrochemical techniques, including Electrochemical Impedance Spectroscopy (EIS) and potentiodynamic polarization. The corroded surfaces of metal samples were examined using an atomic force microscope (AFM). Experimental results revealed that the inhibition efficiency increases with increasing inhibitor content and decreases with increasing temperature. The maximum inhibition efficiency was approximately 90.81%, and was reached in the presence of 0.25 g/L inhibitor at 298 K. The inhibitory action of Lavendula extract was realized via the adsorption of phytochemical constituents on the metal surface. The adsorption follows the Langmuir adsorption mechanism. Thermodynamic parameters suggested that the adsorption was spontaneous at different temperatures, supporting a mixed physisorption and chemisorption mechanism. Electrochemical impedance spectroscopy indicated that the inhibitor ameliorates the film formed at the metal/solution interface. Potentiodynamic polarization studies reveal that the inhibitor behaves as a mixed-type inhibitor, with a predominantly anodic tendency. AFM studies confirmed the adsorption of Lavendula extract on the Monel alloy surface.*

KEYWORDS: *Corrosion; Monel 400; Green inhibitor; Polarization; Electrochemical impedance spectroscopy; Atomic force microscopy.*

**To whom correspondence should be addressed.*

+ E-mail: kh-sihem@hotmail.fr

• Other address: c.

1021-9986/2023/8/2638-2649 12/$/6.02

INTRODUCTION

Corrosion is a spontaneous process that results in the conversion of metals or alloys to a more stable state, by way of their chemical or electrochemical reaction with the environment. It is an undesirable phenomenon in many industrial applications, such as water treatment, acid pickling, and chemical cleaning, as it causes tremendous economic loss and potential safety hazards [1,2]. Monel 400, an alloy of nickel-containing approximately 30-33 wt.% copper, is one of the most preferred alloys for metal construction in many industrial fields, such as marine and chemical processing equipment, due to its excellent mechanical properties. However, in acidic environments, this alloy suffers from selective leaching, wherein nickel is preferentially corroded and removed from the alloy, leading to a porous material with low strength and ductility [3,4]. There exist various methods by which to overcome the corrosive attack caused by acidic solutions, such as coating, use of corrosion inhibitors, and cathodic and anodic protection. In many practical applications, the use of corrosion inhibitors is the most widely used method for corrosion prevention. Unfortunately, the majority of synthetic organic and inorganic inhibitors are toxic to human beings, as well as expensive and environmentally harmful [5,6]. Recently, due to the hazardous environmental effects associated with traditional inhibitors, their use has become limited. Meanwhile, the exploration of naturally-occurring substances as corrosion inhibitors is becoming a field of extensive investigation, due principally to the non-toxic nature and abundance of various active species that can be extracted using simple and economically feasible procedures.

Several plant extracts have been reported as being good corrosion inhibitors for different metals in acidic media [7-10]. The corrosion inhibition effectiveness of these compounds is due to the presence of complex constituents in their composition, such as tannins, flavonoids, alkaloids, polyphenols, and amino acids, which contain heteroatoms with high electron density like nitrogen, phosphorus, oxygen, and sulfur, aromatic rings, and conjugated double bonds [11,12]. The inhibitive action of plant extracts proceeds via the adsorption of their active species on the metal surface, which blocks active sites by displacing adsorbed water molecules at the metal/solution interface, and form a compact barrier film. The adsorbed film acts as a physical barrier, and can prevent metal dissolution by reducing the kinetics of the anodic and/or cathodic reactions of corrosion [13]. The purpose of the present research is to investigate the inhibition effect of Lavandula stoechas, a potential non-toxic corrosion inhibitor for Monel 400 in sulfuric acid (0.5M). The evaluation of corrosion inhibition performance was carried out by weight loss measurements, potentiodynamic and electrochemical impedance spectroscopy (EIS) techniques. The surface morphology was examined using an Atomic Force Microscope (AFM).

EXPERIMENTAL SECTION

Material and electrolyte

The chemical composition (in weight %) of Monel alloy 400 samples used in all experiments was as follows: nickel (min 63%), copper (28–34%), iron (2.5%), manganese (2%), carbon (0.3%), silica (0.5%), sulfur (0.024%). The Monel 400 sheet was cut into dimensions of 10 mm × 10 mm × 4 mm for electrochemical studies, and 20 mm × 10 mm × 4 mm for gravimetric studies. Samples for electrochemical studies were embedded into epoxy resin, leaving an exposed area of 1 cm^2. Prior to all experiments, the exposed surfaces of all specimens were mechanically polished with a series of emery paper grades (240, 400, 600, 800, 1000, and 1200). Then, the specimens were degreased with acetone, washed with distilled water, and dried.

The corrosive electrolyte was sulfuric acid (0.5 M), which was made from H_2SO_4 (analytical Reagent grade 95–97%) and distilled water.

Plant extract preparation

The collected leaves of Lavandula stoechas were dried after rinsing with water, and then pulverised in a hand mill. The obtained leaves' powder (30 g) was macerated in methanol (150 mL) at room temperature for 48 h. The resulting mixture was filtered and concentrated using a rotary evaporator. The main components of the methanolic Lavandula stoechas extract are: flavonoids, apigenin7-glucoside, luteolin, luteolin 7- glucoside, and luteolin 7-glucuronide [14].

Methods

Electrochemical tests

A potentiostat/galvanostat (Voltalab PGZ301) was used for electrochemical tests, and a traditional three- electrode

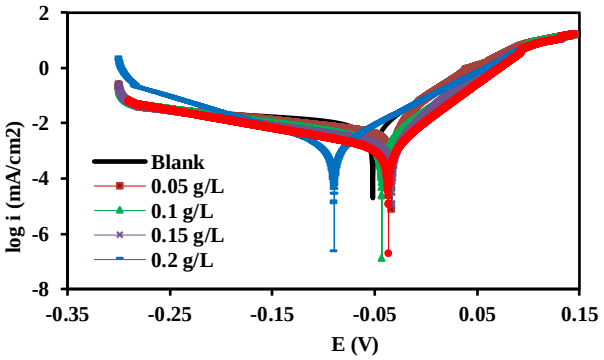

Fig. 1: Polarization curves of Monel 400 measured with different concentrations of Lavandula stoechas extract in 0.5 M H_2SO_4 at 298 K

electrochemical cell was constructed. In the experiments, a prepared Monel specimen was used as the Working Electrode (WE), a platinum electrode was used as the auxiliary electrode (CE), and a Saturated Calomel Electrode (SCE) was used as a reference electrode. After the Open Circuit Potential (OCP) reached the steady state, EIS measurements were carried out, and the potentiodynamic polarization curve was obtained. EIS tests were conducted within the frequency range of 100 kHz to 10 mHz, with an amplitude of 10 mV. The corrosion inhibition efficiency (IE_{Im}%) of the studied inhibitor calculated according to the change in charge transfer resistance (R_{ct}), using Eq. (1) [15]:

$$IE_{EIS}\% = \left[R_{ct} - R^0_{ct}/R_{ct}\right]100 \quad (1)$$

Where R^0_{ct} and R_{ct} are the charge-transfer resistances without and with different concentrations of the extract, respectively.

Polarization curves were measured using a sweep rate of 0.6 mV/s, and the scanning potential range was from −350 mV/(SCE) to +150 mV/(SCE). The inhibition efficiency (IEp%) was estimated from the change in corrosion current density (i_{corr}), as per Eq. (2) [16]:

$$IE_p\% = \left[i^0_{corr} - i_{corr}/i^0_{corr}\right]100 \quad (2)$$

Where i^0_{corr} and i_{corr} are the corrosion current densities of Monel 400 in uninhibited and inhibited solutions, respectively.

Weight loss method

The Monel specimens were immersed for 1h in the test solutions, which were maintained at different temperatures (298–328 K). Before performing the experiment, the Monel coupons were polished and weighed. The cleaned Monel coupons were then immersed in the test solution (100 mL). After immersion, the corroded/inhibited specimens were cleaned, dried in air at room temperature, and then reweighed. The corrosion rate of the specimens was calculated as per Eq. (3) [17]:

$$C_R = \Delta W/A.t \quad (3)$$

Where ΔW is the weight loss of Monel specimens (g), A is the total area of one Monel specimen (cm^2), and t is the immersion time (h). From the corrosion rate thus obtained, the inhibition efficiency (E_G%) and the surface coverage (θ) were calculated according to Eqs. (4) and (5) [18]:

$$E_G\% = \left[C^0_R - C_R/C^0_R\right].100 \quad (4)$$

$$\theta = E_G/100 \quad (5)$$

Where C^0_R and C_R are the corrosion rates of Monel 400 specimens in blank and inhibited corrosive media, respectively.

Surface morphology analysis

The Monel samples were prepared for surface morphology analysis as described in the mass loss measurement section. The polished metal samples were immersed for 24 h in the acidic medium, either without or with the optimum concentration of Lavandula stoechas extract. After cleaning with water and drying, the corroded samples were scanned using a Dimension ICON AFM with Scan Asyst.

RESULTS AND DISCUSSION

Potentiodynamic polarization

Polarization measurements were performed to assess the inhibition performance of the extract and to investigate the kinetics of corrosion reactions. The potentiodynamic polarization curves obtained for Monel 400 in 0.5 M H_2SO_4 solution, without and with various concentrations of inhibitor, are shown in Fig. 1. Kinetic parameters such as corrosion current density (i_{corr}), corrosion potential (E_{corr}), cathodic and anodic Tafel slopes ($ß_c$, $ß_a$), and inhibition efficiency (IE_p%) are illustrated in Table 1. It is clear from Fig. 1, that all cathodic curves display a diffusion-limited plateau region, which is attributed to the oxygen reduction process. By contrast, all anodic curves exhibit well-defined Tafel regions, which may indicate the formation of a non-passive layer

Table 1 : Electrochemical parameters derived from polarization curves for Monel 400 in 0.5 M H_2SO_4 in the absence and presence of Lavandula stoechas extract at 298K

C_{inh} (g/L)	E_{corr}(mV)	i_{corr} (μA/cm^2)	B_a(V/dec)	B_c(V/dec)	IE $_p$ (%)
Blank	-51.788	10.705	53.9	46.6	
0.05	-33.608	4.467	23.9	251.4	58.27
0.1	-42.869	3.104	42.8	199.1	71.00
0.15	-35.679	2.087	30.9	188.8	80.50
0.2	-61.897	1.655	42.6	118.7	84.53
0.25	-36.502	1.311	37.5	155.2	87.75

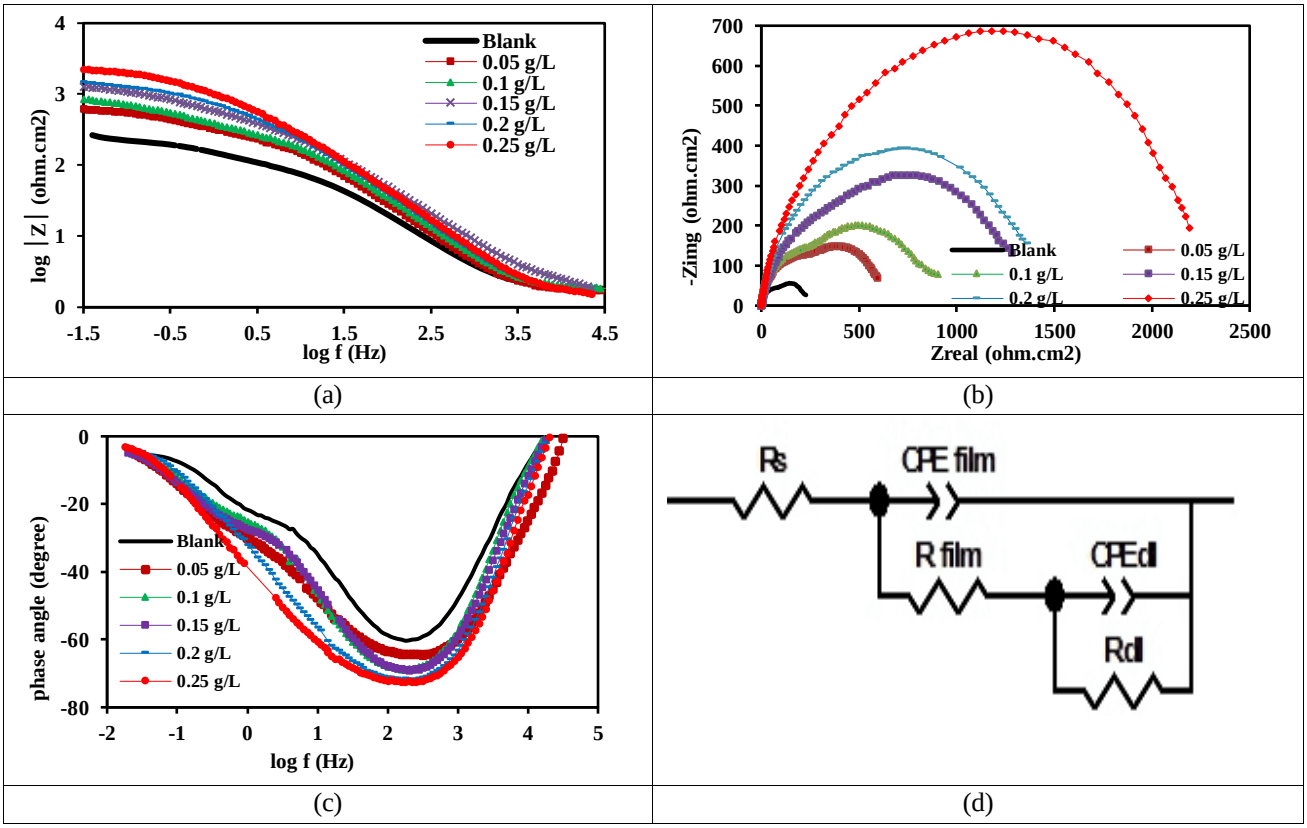

Fig. 2 : Nyquist diagrams (a), bode plots (b), phase plots (c), and fitting circuit (d) of Monel 400 in 0.5M H_2SO_4 in the absence and presence of different concentrations of Lavandula stoechas extract at 298K

formation of a non-passive layer on the metal surface. When comparing the polarization curves of the specimen without or with inhibitor, no significant difference in curve shape can be observed, indicating that the studied green inhibitor can protect the metal without changing the corrosion mechanism. Analysis of the data in Table 1 reveals that the values of E_{corr} are shifted towards a more noble direction in the presence of various concentrations of inhibitor. However, cathodic displacement was only observed at an inhibitor concentration of 0.25 g/L. Furthermore, the maximum variation in E_{corr} with respect to the blank sample is less than 85 mV [19,20]. This observation clearly shows that the Lavandula stoechas extract controls both the anodic and cathodic reactions; thus, acting as a mixed-type inhibitor with a predominantly anodic tendency. The change in β_a and β_c in the inhibited solutions supports the idea that the tested inhibitor controls both the anodic and cathodic reactions. Along these lines, we also observed a decrease in the corrosion current density and an increase in the inhibition efficiency with

Table 2 : Electrochemical parameters of Monel 400 in 0.5 M H_2SO_4 solution without and with Lavandula stoechas extract at 298K

C_{inh}(g/L)	R_s ($\Omega.cm^2$)	CPE_{film} (F/cm^2)	n_1	R_{film} ($\Omega.cm^2$)	CPE_{dl} (F/cm^2)	n_2	R_{tc} ($\Omega.cm^2$)	IE_{EIS} (%)
Blank	1,716	0,00030782	0,84668	92,4	0,00091559	0,791	230,3	
0.05	1,691	0,00016597	0,88198	278,3	0,00059836	0,84031	611,4	62.33
0.1	1,772	0,00012971	0,88081	277,4	0,00056865	0,8493	833,6	72.37
0.15	1,846	0,00017093	0,80825	376	0,00038647	0,78196	1290	82.14
0.2	1,53	0,00015055	0,87293	664,9	0,00036927	0,82919	1669	86.20
0.25	1,547	0,00014989	0,8486	700,4	0,00019318	0,91479	2173	89.40

increasing inhibitor concentration in the acidic medium. The observed inhibitive action of Lavandula stoechas extract can be attributed to the formation of a barrier layer by the adsorbed phytochemical constituents on the metal surface [21].

Electrochemical Impedance Spectroscopy (EIS)

Fig. 2 shows the Nyquist and Bode plots of Monel 400 in 0.5M H_2SO_4, both in the absence and presence of various concentrations of Lavandula stoechas extract. It can be seen that the Nyquist diagrams are characterised by a flattened, semi-circular shape. This behavior is due to frequency dispersion, induced by the roughness and inhomogeneity of the metal surface. It can also be observed in Fig. 2(a) that the radius of the capacitive loop of the inhibited substrate increased with the concentration of corrosion inhibitor. These observations clearly suggest the adsorption of inhibitor molecules onto the active sites of the metal surface [22]. On the other hand, it is clear from the Bode modulus diagram (Fig. 2(b)) that the impedance modulus at low frequencies increases with inhibitor concentration, compared to that of the blank electrode. The shift of |Z| may be attributed to the formation of a protective layer on the Monel surface [23,24]. It is also clear from the phase angle curves (Fig. 2(c)), that the experimental spectra experience two relaxation processes. The low-frequency relaxation process is referred to the charge transfer process, and the high-frequency process is related to the adsorption of the inhibitor at the metal/solution interface. In addition, the effect of the inhibitor on the Monel surface is clearly detectable in the high-frequency domain. It can be seen that the addition of Lavandula stoechas extract to the electrolyte in these tests increases the maximum phase angle of the high-frequency constant time. The increase in phase angle with inhibitor concentration reveals a decrease in the surface roughness, as a result of the enlarged surface coverage.

According to the Nyquist and Bode plots, the equivalent circuit with two time constants (Fig. 2(d)) was adopted to simulate the obtained EIS. In the proposed model, R_s, R_f, and R_{ct} are the resistances relative to the corrosive electrolyte, the oxide layer formed on the metallic surface, and the charge transfer process in the double layer, respectively. Q_f and Q_{dl} are the Constant Phase Elements (CPE) of the corrosion product and the double layer, respectively. CPE is used as a substitute for of pure capacitance, owing to the non-ideal performance of the working electrode [25]. CPE can be expressed as per Eq. (6) [26]:

$$Z_{CPE}=Y_0^{-1}(jw)^{-n} \quad (6)$$

where Z_{CPE} is the impedance of CPE, j is an imaginary unit, ω is the angular frequency, Y_0 is a constant, and n is the dispersion coefficient. Generally, in the case of n = 0, -1, +1, and ½, the CPE represents a pure resistor, an inductor, a pure capacitor, or Warburg impedance, respectively [27].

The electrochemical impedance parameters found from analysis of the Nyquist diagram are listed in Table 2. It can be seen from this table that the both CPE_{film} and CPE_{dl} are reduced, while R_f and R_{ct} increase after the addition of Lavandula stoechas. This phenomenon may be attributed to an increase in the insulating performance of the double layer, as a result of inhibitor adsorption. Thus, adsorption of more inhibitor species as the inhibitor dose increases results in a further increase in the thickness of the electrical double layer, and/or a decrease in the local dielectric constant [28,29]. The calculated inhibition efficiency follows a similar trend to the polarization measurements, reaching a maximum of 89.40% in the presence of 0.25 g/L of Lavandula stoechas extract.

Weight loss measurements

The assessment of the corrosion inhibition of Monel 400 by Lavandula stoechas extract was also conducted

Table 3: Weight loss parameters for Monel alloy 400 in 0.5 M H_2SO_4 containing Lavandula stoechas extract

C_{inh} (g/L)	C_R (g.cm^{-2}h)	E_G%	θ
0	1.84 10^{-5}		
0.05	7.08 10^{-6}	61.50	0.615
0.1	4.93 10^{-6}	73.20	0.732
0.15	3.04 10^{-6}	83.47	0.8347
0.2	2.31 10^{-6}	87.40	0.874
0.25	1.69 10^{-6}	90.77	0.9077

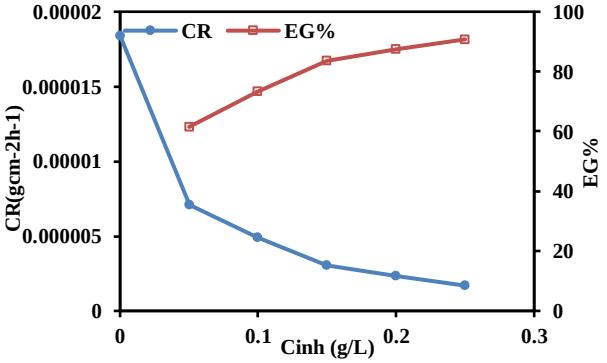

Fig. 3: Corrosion rate and inhibition efficiency of Monel 400 specimens in 0.5 M H_2SO_4 with and without Lavandula extract using the weight loss method

using the gravimetric method, due to its ease of implementation and good reliability. This was performed by immersing Monel 400 specimens in H_2SO_4 (0.5 M) solution containing varying concentrations of inhibitor for 1h at room temperature (298 K). The parameters calculated from gravimetric measurements, in terms of corrosion rate (C_R), inhibition efficiency (E_G%), and surface coverage (θ), are summarised in Table 3. It can be seen here that, with enhancing inhibitor concentration in the solution, the corrosion rate of Monel 400 decreases and the inhibition efficiency increases. The increase in inhibition efficiency with increasing inhibitor concentration is a consequence of the increased number of adsorbed Lavandula phytochemicals' constituents on the metal surface, and the subsequent formation of a protective barrier that isolates the active sites of the metallic surface from the active species in the test solution [30,31]. A plot of inhibition efficiency vs. inhibitor concentration (Fig. 3) shows that the maximum efficiency (90.77%) was recorded when 0.25 g/L Lavandula extract concentration was used.

Effect of temperature

The influence of temperature on the corrosion of Monel 400 in 0.5 M H_2SO_4 was investigated, at temperatures ranging from 298 to 328K. The calculated data are displayed in Table 4. It can be seen that an increase in the temperature of the solution increases the corrosion rate of both the uninhibited and inhibited samples, and results in a slight decrease in corrosion inhibition efficiency and surface coverage. The decrease in inhibitor performance as the temperature rises is due to electrostatic interaction between the inhibitor molecules and the metal surface [32].

Activation and thermodynamic parameter calculations

The kinetic corrosion parameters of Monel alloy 400 in 0.5 M H_2SO_4 before and after adding the studied extract can be calculated by Arrhenius (Eq. (7)) and transition state equations (Eq. (8)) [33,34]:

$$\log(C_R) = -E_a/2.303\ RT + k \quad (7)$$

$$\log(C_R/T) = [\log(R/Nh) + (\Delta S_a/2.303\ R)] - [\Delta H_a/2.303\ RT] \quad (8)$$

Where E_a is the activation energy, R is the universal gas constant, T is the absolute temperature, k is the Arrhenius constant, h is Planck's constant, N is Avogadro's number, ΔH_a is the activation enthalpy, and ΔS_a is activation entropy.

The values of E_a were calculated from the slopes of the plot ln C_R vs. $10^3/T$ (Fig. 4). ΔS_a and ΔH_a values were calculated from the slopes and intercepts of the plot ln (C_R/T) vs. $10^3/T$ (Fig. 5). The calculated values of the kinetic parameters are summarised in Table 5. From this table, it can be seen that the E_a values of the inhibited specimens are higher than those of the uninhibited specimen. This result indicates the inhibitor's ability over the entire range of temperatures tested to create a protective barrier against corrosion [35,36]. The positive values of ΔH_a in inhibited and uninhibited solutions suggest that the corrosion process is endothermic [37]. The

Table 4: Corrosion rate and corresponding inhibition efficiency for the corrosion of Monel 400 in 0.5 H_2SO_4 without and with various concentrations of Lavandula stoechas extract at different temperatures.

T (K)	C_{inh} (g.L)	C_R (g. $cm^{-2}h^{-1}$)	E_G%	θ
298	Blank	0,0000184		
	0.05	0,00000708	61.52	0.6152
	0.1	0,00000493	73.20	0.7320
	0.15	0,00000304	83.47	0.8347
	0.20	0,00000231	87.44	0.8744
	0.25	0,00000169	90.81	0.9081
308	Blank	0,0000436		
	0.05	0,0000176	59.63	0.8563
	0.1	0,0000131	69.95	0.6995
	0.15	0,00000773	82.27	0.8227
	0.20	0,00000632	85.5	0.855
	0.25	0,00000484	88.89	0.8889
318	Blank	0,0000503		
	0.05	0,0000209	58.44	0.5844
	0.1	0,0000170	66.20	0.6620
	0.15	0,00000992	80.27	0.8027
	0.20	0,00000792	84.25	0.8425
	0.25	0,00000622	87.63	0.8763
328	Blank	0,0000645		
	0.05	0,0000313	51.47	0.5147
	0.1	0,00002867	55.55	0.5555
	0.15	0,0000226	64.96	0.6496
	0.20	0,0000206	68.06	0.6806
	0.25	0,0000180	72.05	0.7205

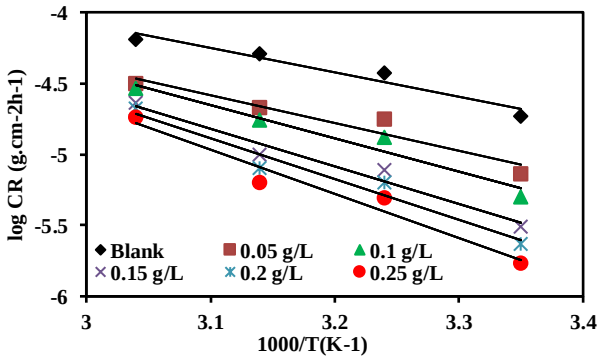

Fig. 4 : Arrhenius plots for Monel 400 corrosion in 0.5 M H_2SO_4 solution with different concentrations of Lavandula stoechas extract

results show that the entropies of activation are negative both in the absence and presence of the investigated inhibitor, and exhibit a gradual increase as the inhibitor content is increased. The negative values of ΔS_a imply that the system crosses from an ordered to a more disordered arrangement. The increase in disorder can be ascribed to the replacement process of water molecules during the adsorption of inhibitor molecules on the metal surface [38].

Adsoption isotherm

Adsorption isotherm studies play a reliable role in understanding the interaction between the metal surface and inhibitor molecules. Various isotherms, such as Langmuir, Freundlich, Frumkin, Temkin, El-Awady, and Flory-Huggins, have been evaluated in an attempt to clarify the adsorption behavior of Lavandula stoechas extract. However, the best agreement was obtained using the Langmuir adsorption isothermal equation, as follows (Eq. (9)) [39]:

$$C_{inh}/\theta=[1/K_{ads}]+C_{inh} \quad (9)$$

Table 5: Activation parameters of Monel 400 in the presence of Lavandula stoechas extract at different concentrations in 0.5 M H_2SO_4 solution

C_{inh} (g/L)	E_a (kJ.mol^{-1})	ΔH_a (kJ.mol^{-1})	ΔS_a (J.mol^{-1}K^{-1})
Blank	32.871	34.403	-217
0.05	37.395	34.799	-223
0.1	44.764	42.755	-200
0.15	50.617	48.217	-186.5
0.2	54.88	52.307	-175
0.25	59.524	56.548	-163

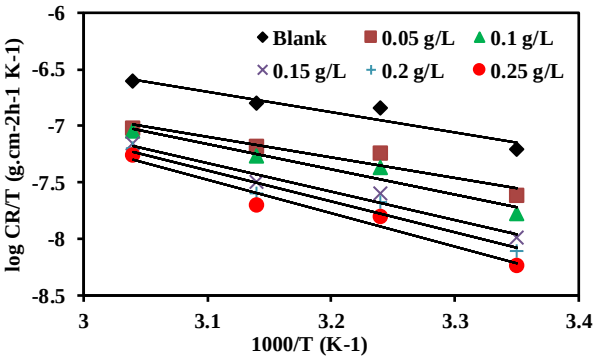

Fig. 5: Transition-state of Monel 400 corrosion in 0.5 M H_2SO_4 solution with various concentrations of Lavandula stoechas extract

Where C_{inh} is the inhibitor concentration and K_{ads} is the adsorption equilibrium constant for the adsorption/desorption process. As displayed in Fig. 6, plotting C_{inh} vs. C_{inh}/θ reveals a linear relationship. The strong correlation ($R^2 >$ 0.99) indicates that the adsorption of the investigated inhibitor on the metal surface fully obeys this isotherm. The Langmuir adsorption isotherm assumes that the adsorbed species occupy only one surface site and that there are no interactions with other adsorbed species [40,41].

The standard adsorption free energy (ΔG^0_{ads}) of the inhibitor molecules can be calculated according to Eq. (10) [42]:

$$\Delta G^0_{ads} = -RT\ln(1000K_{ads}) \quad (10)$$

Where *1000* refers to the mass concentration of water molecules in the solution (g/L). The calculated values of ΔG^0_{ads} are reported in Table 6. Negative values for ΔG^0_{ads} indicate that the adsorption of the inhibitor molecules on the Monel surface is a spontaneous process [43]. It is generally considered that the adsorption type is regarded as physisorption if the value of ΔG^0_{ads} is less negative

Table 6: Langmuir adsorption fitting and thermodynamic adsorption parameters for Lavandula stoechas adsorption at various temperatures

T (K)	R^2	K_{ads} (L/g)	ΔG^0_{ads} (kJ/mol)
298	0.999	27.855	-25.34
308	0.998	26.954	-25.25
318	0.991	25.974	-25.17
328	0.990	25.641	-25.14

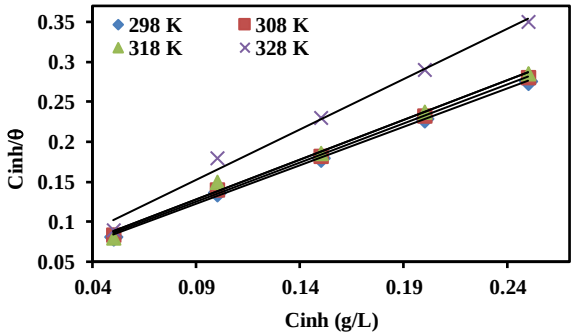

Fig. 6: Langmuir isotherm for adsorption of Lavandula stoechas extract onto Monel 400 surface in 0.5 M H_2SO_4 at different temperatures

than-20 kJ/mol. The adsorption mechanism is due to the electrostatic interaction between the charged metal and inhibitor molecules. When the absolute value of ΔG^0_{ads} is more negative than –40 kJ/mol, the adsorption may be considered as chemisorption, which involves the sharing of electron pairs between heteroatoms or π–electrons of aromatic rings to form rigid, coordinated bonds [44]. For the adsorption system in this work, the calculated values of ΔG^0_{ads} were between –20 and –40 kJ/mol, confirming that the inhibitor adsorbs on the Monel surface by electrostatic and chemically-interactive processes [45].

Atomic Force Microscopy (AFM) characterization

The surface texture of Monel alloy 400 samples was studied using AFM. Fig. 7 shows the three-dimensional (3D) AFM micrographs of Monel 400: (a) after immersion in 0.5 M H_2SO_4 without inhibitor, and (b) with 0.25 g/L of inhibitor for 24 h, under atmospheric conditions. The (3D-a) image shows that the surface of the Monel 400 electrode dipped in the uninhibited solution was damaged drastically. In contrast, in the solution containing 0.25 g/L of inhibitor, AFM analysis of the Monel alloy reveals a smooth surface (3D-b). The reduction in surface damage can be explained by the adsorption of inhibitor molecules on the metal surface.

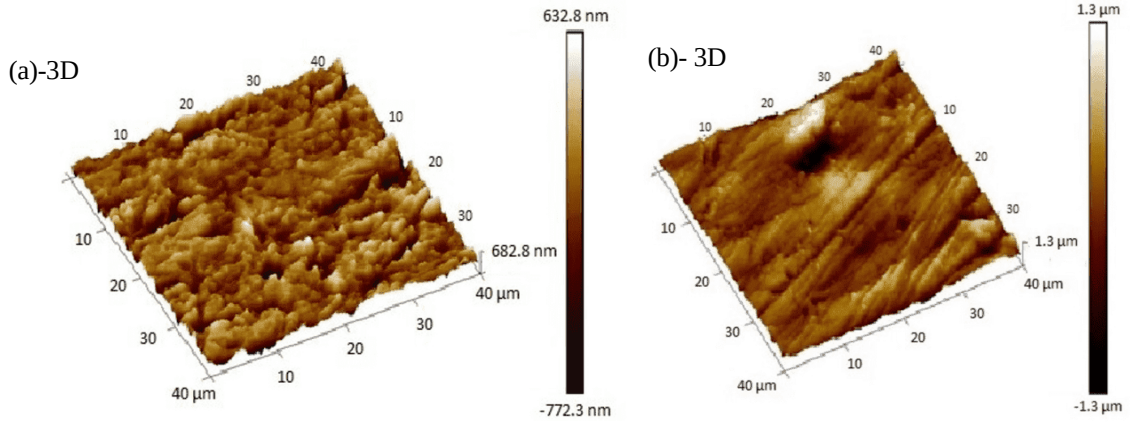

Fig. 7: AFM images in 3-D formats for Monel alloy 400 after immersion in 0.5 H_2SO_4 solution (a) without and with (b) Lavandula stoechas for 24 h under normal atmospheric condition

CONCLUSIONS

The inhibition performance and adsorption behavior of Lavandula stoechas as a green corrosion inhibitor for Monel alloy 400 in 0.5M H_2SO_4 solution were evaluated via gravimetric method, electrochemical techniques, and surface analysis. The results obtained led to the following conclusions:

- Weight loss measurements and electrochemical investigations showed that Lavandula stoechas extract was an effective inhibitor against Monel 400 corrosion in 0.5M H_2SO_4 solution. The extract's anticorrosive effectiveness was found to increase with concentration and decrease with increasing temperature. The maximum inhibition efficiency of 90.81% was obtained at 298 K, at an inhibitor concentration of 0.25 g/L.
- The inhibition performance of Lavandula stoechas extract is mainly due to the formation of a protective layer via the adsorption of its phytochemical constituents on the metal surface. The adsorption isotherm illustrates that the process fits well the Langmuir monomolecular adsorption model. The thermodynamic parameters calculated from the weight loss results showed that the adsorption process of Lavandula stoechas extract is spontaneous, and may proceed through both physisorption and chemisorption mechanisms.
- EIS measurements show two time constants, which are attributed to the faradaic process and the adsorbed protective layer on the metal surface.
- The potentiodynamic polarization measurements reveal that the tested extract behaves as a mixed-type corrosion inhibitor, which adsorbs onto the metal and reduces both anodic and cathodic kinetics.
- AFM morphology analysis proved that Lavandula stoechas can effectively adsorb onto the metal surface, and reduce the corrosion rate of Monel 400 in 0.5 M sulfuric acid.

Nomenclature

θ	surface coverage
ΔH_a	activation enthalpy
ΔS_a	activation entropy
i^0_{corr}	corrosion current density in uninhibited solution
R^0_{ct}	charge-transfer resistances in unhibited solution
ΔG^0_{ads}	standard adsorption free energy
A	Surface
AFM	atomic force microscope
$C^0{}_R$	corrosion rates in blank solution
C_{inh}	inhibitor concentration
CPE	constant phase elements
C_R	corrosion rates in inhibited solution
E%	inhibition efficiency
E_a	activation energy
E_{corr}	corrosion potential
EIS	electrochemical impedance spectroscopy
i_{corr}	corrosion current density in inhibited medium
j	imaginary unit
k	Arrhenius constant
K_{ads}	adsorption equilibrium constant
n	dispersion coefficient

N	Avogadro's number
Q_{dl}	constant phase elements of the double layer
Q_f	constant phase elements of corrosion product
R	universal gas constant
R^2	Correlation coefficient
R_{ct}	charge-transfer resistances in inhibited solution
R_f	resistances of the oxide layer
R_s	resistances of the corrosive electrolyte
$ß_a$	anodic Tafel slope
$ß_c$	cathodic Tafel slope
T	the absolute temperature
Y_0	Constant
Z_{CPE}	impedance of CPE
ΔW	weight loss
ω	angular frequency

Received : Oct.18, 2022 ; Accepted : Jan. 30, 2023

REFERENCES

[1] Zhang M., Guo L., Zhu M., Wang K., Zhang R., He Z., Lin Y., Leng S., Anadebe V.C., Zheng X., Akebia Trifoliate Koiaz Peels Extract as Environmentally Benign Corrosion Inhibitor for Mild Steel in HCl Solutions: Integrated Experimental and Theoretical Investigations, *J. Ind. Eng. Chem.*, **101**: 227-236 (2021).

[2] Dehghani A., Bahlakeh G., Ramezanzadeh B., A Detailed Electrochemical/Theoretical Exploration of the Aqueous Chinese Gooseberry Fruit Shell Extract as a Green and Cheap Corrosion Inhibitor for Mild Steel in Acidic Solution, *J Mol Liq.*, **282**: 366-384 (2019).

[3] El Din A.M.S., Dahshan M.E.E., Taj El Din A.M., Dissolution of Copper and Copper-Nickel Alloys in Aerated Dilute HCl Solutions, *Desalination*, **130**: 89-97 (2000).

[4] Singh V.B., Gupta A., The Electrochemical Corrosion and Passivation Behaviour of Monel (400) in Concentrated Acids and Their Mixtures, *J. Mater. Sci.*, **36**: 1433-1442 (2001).

[5] Wang D., Li Y., Chang T., Luo A., Experimental and Theoretical Studies of Chitosan Derivatives as Green Corrosion Inhibitor for Oil and Gas Well Acid Acidizing, *Colloids Surf. A Physicochem. Eng.*, **628**: 127308 (2021).

[6] Zhang Q.H., Hou B.S., Li Y.Y., Lei Y., Wang X., Liu H F., Zhang G.A., Two Amino Acid Derivatives as High Efficient Green Inhibitors for the Corrosion of Carbon Steel in CO_2-Saturated Formation Water, *Corros. Sci.*, **189** : 109596 (2021).

[7] Sun X., Qiang Y., Hou B., Zhu H., Tian H., Cabbage Extract as an Eco-Friendly Corrosion Inhibitor for X70 Steel in Hydrochloric Acid Medium, *J. Mol. Liq.*, **362**: 119733 (2022).

[8] Prifiharni S., Mashanafie G., Priyotomo G., Royani A., Ridhova A., Elya B., Soedarsono, J.W., Extract Sarampa Wood (Xylocarpus Moluccensis) as an Eco-Friendly Corrosion Inhibitor for Mild Steel In HCl 1M, *J. Indian Chem. Soc.*, **99(7)**: 100520 (2022).

[9] Wan S., Wei H., Quan R., Luo Z., Wang H., Liao B., Guo X., Soybean Extract Firstly Used as a Green Corrosion Inhibitor with High Efficacy and Yield for Carbon Steel in Acidic Medium, *Ind. Crops Prod.*, **187**: 115354 (2022).

[10] Wang Q., Zheng H., Liu L., Zhang Q., Wu X., Yan Z., Sun Y., Li X., Insight into the Anti–Corrosion Behavior of Reineckia Carnea Leaves Extract as an Eco–Friendly And High–Efficiency Corrosion Inhibitor, *Ind. Crops Prod.*, **188**: 115640 (2022).

[11] Hossain N., Chowdhury M.A., Iqbal A.P., Islam M.S., Omar N.Y.S., Saifullah A.Z.A., Paederia Foetida Leaves Extract as a Green Corrosion Inhibitor for Mild Steel in Hydrochloric Acid Solution, *Curr. Res. Green Sustainable Chem.*, **4**: 100191 (2021).

[12] Hajsafari N., Razaghi Z., Tabaian S.H., Electrochemical Study and Molecular Dynamics (MD) Simulation of Aluminum in the Presence of Garlic Extract as a Green Inhibitor, *J. Mol. Liq.*, **336**: 116386 (2021).

[13] Mobtaker H., Azadi M., Hassani N., Neek-Amal M., Rassouli M., Bidi M.A., The Inhibition Performance of Quinoa Seed on Corrosion Behavior of Carbon Steel in the HCl Solution; Theoretical and Experimental Evaluations, *J. Mol. Liq.*, **335**: 116183 (2021).

[14] Dif M.M., Benyahia M., Benali F.T., Rahmani M., Bouazza S., Phenolic Content and Antioxidant Activity of Three Algerian Species of Lavenders, *Phytothérapie*, **15**: 367-372 (2017).

[15] Li Y., Chen H., Tan B., Xiang B., Zhang S., Luo W., Zhang Y., Zhang J., Three Piperazine Compounds as Corrosion Inhibitors for Copper in 0.5 M Sulfuric Acid Medium, *J. Taiwan Inst. Chem. Eng.*, **126**: 231-243 (2021).

[16] Lu Y., Zhou L., Tan B., Xiang B., Zhang S., Wei S., Wang B., Yao Q., Two Common Antihistamine Drugs as High-Efficiency Corrosion Inhibitors for Copper in 0.5 M H_2SO_4, *J. Taiwan Inst. Chem. Eng.*, **123**: 11-20 (2021).

[17] Li X., Deng S., Du G., Xie X., Synergistic Inhibition Effect of Walnut Green Husk Extract and Sodium Lignosulfonate on the Corrosion of Cold Rolled Steel in Phosphoric Acid Solution, *J. Taiwan Inst. Chem. Eng.*, **114**: 263-283 (2020).

[18] Silva E.F., Wysard J.S., Bandeira M.C., Mattos O.R., Electrochemical and Surface Enhanced Raman Spectroscopy Study of Guanine as Corrosion Inhibitor for Copper, *Corros. Sci.*, **191**: 109714 (2021).

[19] Chen Z., Wang M., Fadhil A.A., Fu C., Chen T., Chen M., Khadom A.A., Mahood H.B., Preparation, Characterization, and Corrosion Inhibition Performance of Graphene Oxide Quantum Dots for Q235 Steel in 1 M Hydrochloric Acid Solution, *Colloids Surf. A Physicochem. Eng.*, **627**: 127209 (2021).

[20] Wang D., Li Y., Chen B., Zhang L., Novel Surfactants as Green Corrosion Inhibitors for Mild Steel in 15% HCl: Experimental and Theoretical Studies, *Chem. Eng. J.*, **402**: 126219 (2020).

[21] Tehrani M.E.H.N., Ghahremani P., Ramezanzadeh M., Bahlakeh G., Ramezanzadeh B., Theoretical and Experimental Assessment of a Green Corrosion Inhibitor Extracted from Malva Sylvestris, *J. Environ. Chem. Eng.*, 9: 105256 (2021).

[22] Kahkesh H., Zargar B., Corrosion Protection Evaluation of Allium Jesdianum as a Novel and Green Source Banner for Mild Steel in 1M HCl Solution, *J. Mol. Liq.*, **344**: 117768 (2021).

[23] Thaha Y.N., Kartika I., Astawa I.N.G.P., Lestari F.P., Eryani A., Rokhmanto F., Utomo M.S., The Effects of Na_2HPO_4 on Corrosion Behaviour of Mg–5% Zn and Mg–7% Zn Alloys in Ovalbumin, *Mater. Chem. Phys.*, **273**: 125112 (2021).

[24] Mishra P., Yavas D., Bastawros A.F., Hebert K.R., Electrochemical Impedance Spectroscopy Analysis of Corrosion Product Layer Formation on Pipeline Steel, *Electrochim. Acta.*, **346**: 136232 (2020).

[25] Ma Y., Xiong H., Chen B., Effect of Heat Treatment on Microstructure and Corrosion Behavior of Mg-5Al-1Zn-1Sn Magnesium Alloy, *Corros. Sci.*, **191**: 109759 (2021).

[26] Wang Q., Cao X., Wu T., Liu M., Li C., Yin F., Corrosion of X80 Steel Welded Joint Under Disbonded Coating in an Acidic Soil Solution, *Int. J. Pressure Vessels Piping.*, **194**: 104508 (2021).

[27] Huang L., Wang S.S., Li H.J., Wang J.Y., Li Z.G., Wu Y.C., Highly Effective Q235 Steel Corrosion Inhibition in 1M HCl Solution by Novel Green Strictosamide from Uncaria Laevigata: Experimental and Theoretical Approaches, *J. Environ. Chem. Eng.*, **10**: 107581 (2022).

[28] Rajamohan N., Al Shibli F.S.Z.S., Rajasimman M., Environmentally Benign Prosopis Juliflora Extract for Corrosion Protection by Sorption-Gravimetric, Mechanistic and Thermodynamic Studies, *Environ. Res.*, **203**: 111816 (2022).

[29] Abou-Elseoud W.S., Abdel-karim A.M., Hassan E.A., Hassan M.L., Enzyme-and Acid-Extracted Sugar Beet Pectin as Green Corrosion Inhibitors for Mild Steel in Hydrochloric Acid Solution, *Carbohydr. Polym. Technol. Appl.*, **2**: 100072

[30] El-Zekred M.A., Nofal A.M., Shalabi K., Fouda A.S., Ficus Carica Extract as Environmentally Friendly Inhibitor for the Corrosion of L-80 Carbon Steel in 0.5 M H_2SO_4 Media, *J. Indian Chem. Soc.*, **98**: 100128 (2021).

[31] Thomas A., Prajila M., Shainy K.M., Joseph A., A Green Approach to Corrosion Inhibition of Mild Steel in Hydrochloric Acid Using Fruit Rind Extract of Garcinia Indica (Binda), *J. Mol. Liq.*, **312**: 113369 (2020).

[32] Fernandes C.M., Pina V.G., Alvarez L.X., de Albuquerque A.C.F., dos Santos Júnior F.M., Barrios A.M., Velasco J.A., Ponzio E.A., Use of a Theoretical Prediction Method and Quantum Chemical Calculations for the Design, Synthesis and Experimental Evaluation of Three Green Corrosion Inhibitors for Mild Steel, *Colloids Surf. A Physicochem. Eng.*, **599**: 124857 (2020).

[33] Fernine Y., Ech-chihbi E., Arrousse N., El Hajjaji F., Bousraf F., Ebn Touhami M., Rais Z., Taleb M., Ocimum Basilicium Seeds Extract as an Environmentally Friendly Antioxidant and Corrosion Inhibitor for Aluminium Alloy 2024-T3 Corrosion in 3 Wt% NaCl Medium, *Colloids Surf. A Physicochem. Eng.*, **627**: 127232 (2021).

[34] Sanumi O.J., Saliu O.D., Makhatha M.E., Alternative Surface Localization Studies and Electrochemical Investigation of Tyrosine Hybridized Poly (Ethylene Glycol) for Corrosion Inhibition of Mild Steel, *J. Mater. Res. Technol.*, **13**: 700-715 (2021).

[35] Chen Z., Fadhil A.A., Chen T., Khadom A.A., Fu C., Fadhil N.A., Green Synthesis of Corrosion Inhibitor With Biomass Platform Molecule: Gravimetrical, Electrochemical, Morphological, and Theoretical Investigations, *J Mol Liq.*, **332**: 115852 (2021).

[36] Zhang Q.H., Hou B.S., Li Y.Y., Zhu G.Y., Lei Y., Wang X., Liu H.F., Zhang G.A., Dextran Derivatives as Highly Efficient Green Corrosion Inhibitors for Carbon Steel in CO_2-Saturated Oilfield Produced Water: Experimental and Theoretical Approaches, *Chem. Eng. J.*, **424**: 130519 (2021).

[37] Jmiai A., Tara A., El Issami S., Hilali M., Jbara O., Bazzi L., A New Trend in Corrosion Protection of Copper in Acidic Medium by Using Jujube Shell Extract as an Effective Green and Environmentally Safe Corrosion Inhibitor: Experimental, Quantum Chemistry Approach and Monte Carlo Simulation Study, *J Mol Liq.*, **322**: 114509 (2021).

[38] Zakaria K., Abbas M.A., Bedair M.A., Herbal Expired Drug Bearing Glycosides and Polysaccharides Moieties as Green and Cost-Effective Oilfield Corrosion Inhibitor. Electrochemical and Computational Studies, *J. Mol. Liq.*, **352**: 118689 (2022).

[39] Aslam R., Mobin M., Obot I.B., Alamri A.H., Ionic Liquids Derived From A-Amino Acid Ester Salts as Potent Green Corrosion Inhibitors for Mild Steel in 1M HCl, *J Mol Liq.*, **318** : 113982 (2020).

[40] Hassan R.M., Ibrahim S.M., Performance and Efficiency of Methyl-Cellulose Polysaccharide as a Green Promising Inhibitor for Inhibition of Corrosion of Magnesium in Acidic Solutions, *J. Mol. Struct.*, 1246: **131180** (2021).

[41] Abdallah M., Altass H.M., Al-Gorair A.S., Al-Fahemi J.H., Jahdaly B.A.A.L., Soliman K.A., Natural Nutmeg Oil as a Green Corrosion Inhibitor for Carbon Steel in 1.0 M HCl Solution: Chemical, Electrochemical, and Computational Methods, *J. Mol. Liq.*, **323**: 115036 (2021).

[42] Zhang W., Nie B., Wang M., Shi S., Gong L., Gong W., Pang H., Liu X., Li B., Feng Y., Wu Y.C., Chemically Modified Resveratrol as Green Corrosion Inhibitor for Q235 Steel: Electrochemical, SEM, UV and DFT Studies, *J. Mol. Liq.*, **343**: 117672 (2021).

[43] Ye Y., Yang D., Chen H., A Green and Effective Corrosion Inhibitor of Functionalized Carbon Dots, *J. mater. Sci. Technol.*, **35**: 2243-2253 (2019).

[44] Saraswat V., Yadav M., Improved Corrosion Resistant Performance of Mild Steel under Acid Environment by Novel Carbon Dots as Green Corrosion Inhibitor, *Colloids Surf. A Physicochem. Eng.*, **627**: 127172 (2021).

[45] Koundal M., Singh A.K., Sharma C., Study on the Effect of Imidazolium Ionic Liquid as a Modulator of Corrosion Inhibition of Anionic Surfactant Sodium Dodecyl Sulfate (SDS) on Mild Steel in Sodium Chloride Solution, *J. Mol. Liq.*, **350**: 118561 (2022).

.